ARL-TR-8790 ● SEP 2019

DEVCOM ARMY RESEARCH LABORATORY

Noise Photons Due to Self-Phase Modulation in an Entangled Photon Source

by Alexandra Morosova, Daniel E Jones, and Michael Brodsky

NOTICES

Disclaimers

The findings in this report are not to be construed as an official Department of the Army position unless so designated by other authorized documents.

Citation of manufacturer's or trade names does not constitute an official endorsement or approval of the use thereof.

Destroy this report when it is no longer needed. Do not return it to the originator.

ARL-TR-8790 ● SEP 2019

Noise Photons Due to Self-Phase Modulation in an Entangled Photon Source

by Daniel E Jones and Michael Brodsky
Computational and Information Sciences Directorate, CCDC Army Research Laboratory

Alexandra Morosova
Bergen County Academies [Internship]

REPORT DOCUMENTATION PAGE

Form Approved
OMB No. 0704-0188

1. REPORT DATE *(DD-MM-YYYY)*	2. REPORT TYPE	3. DATES COVERED (From - To)
September 2019	Technical Report	1 July–30 August 2019

4. TITLE AND SUBTITLE
Noise Photons Due to Self-Phase Modulation in an Entangled Photon Source

5a. CONTRACT NUMBER

5b. GRANT NUMBER

5c. PROGRAM ELEMENT NUMBER

6. AUTHOR(S)
Alexandra Morosova, Daniel E Jones, and Michael Brodsky

5d. PROJECT NUMBER

5e. TASK NUMBER

5f. WORK UNIT NUMBER

7. PERFORMING ORGANIZATION NAME(S) AND ADDRESS(ES)
CCDC Army Research Laboratory
ATTN: FCDD-RLC-NT
Adelphi, MD 20783

8. PERFORMING ORGANIZATION REPORT NUMBER
ARL-TR-8790

9. SPONSORING/MONITORING AGENCY NAME(S) AND ADDRESS(ES)

10. SPONSOR/MONITOR'S ACRONYM(S)

11. SPONSOR/MONITOR'S REPORT NUMBER(S)

12. DISTRIBUTION/AVAILABILITY STATEMENT
Approved for public release; distribution is unlimited.

13. SUPPLEMENTARY NOTES
ORCID ID: Daniel Jones, 0000-0002-9854-5767

14. ABSTRACT

The distribution of entanglement over a network is essential for performing quantum networking applications. However, available (or technologically feasible) entangled photon sources output not only pairs of entangled photons, but also various types of noise photons, which hinder the ability to successfully distribute entanglement. Quantum network operators must know exactly what types of photons their entangled sources are creating to effectively distribute entanglement over the network. In this report, we describe precisely timed measurements of detection events and the resulting ratio of coincidental to accidental detections, known as the coincidence to accidental ratio (CAR). We then perform a nonlinear regression on the CAR data to prove that the accidental coincidences due to noise in our setup scale stronger than quadratically in pump power. We are able to fit some of the data with an analytical model, which provides evidence of an additional source of noise due to self-phase modulation of the pump laser.

15. SUBJECT TERMS
quantum networks, quantum communications, entanglement, entangled photon sources, self-phase modulation

16. SECURITY CLASSIFICATION OF:			17. LIMITATION OF ABSTRACT	18. NUMBER OF PAGES	19a. NAME OF RESPONSIBLE PERSON
a. REPORT	b. ABSTRACT	c. THIS PAGE			Daniel Jones
Unclassified	Unclassified	Unclassified	UU	23	19b. TELEPHONE NUMBER (Include area code) 301-394-0503

Standard Form 298 (Rev. 8/98)
Prescribed by ANSI Std. Z39.18

Contents

List of Figures

Acknowledgments

Research was sponsored by the US Army Combat Capabilities Development Command Army Research Laboratory and performed with a high school intern (Alexandra Morosova).

1. Introduction

Quantum networks provide many potential applications in communications and computing that cannot be performed with classical networks.[1,2] However, significant progress must be made before large-scale quantum networks can be built to realize these applications. In general, such a network will fundamentally require the capability to create, manipulate, store, and potentially distribute quantum states. Therefore, a quantum network must be developed in which quantum channels[3] are used to transmit quantum states between the nodes where quantum states are created, manipulated, and stored.[4,5] Entangled states of photons traversing the network are one type of state of particular interest for developing a quantum network. Such entangled states exhibit stronger-than-classical correlations between two photons, which can be used as a resource for many quantum networking applications. Ideally, network nodes would include perfect entangled photon sources (EPSs) that distribute many perfectly entangled photons and no additional noise photons; however, such an EPS does not exist. Therefore, it follows that users of a quantum network require intimate knowledge of exactly what types of photons their entangled sources are creating and sending over the network.

In this technical report, we describe several important measurement processes required to operate and characterize the behavior of the NuCrypt entangled photon distribution system[6] located in the Army Research Laboratory (ARL) Quantum Network Testbed. First, we explain the experimental setup, which consists of a NuCrypt EPS, two polarization analyzers (PAs), and a correlated photon detection system (CPDS). Next, we detail the process of characterizing the spectrum of entangled photons output by the EPS. Then we explain the processes required to characterize the behavior of the source by measuring the coincidence to accidental ratio (CAR) of light output by the EPS, by performing quantum state tomography, and by analyzing the concurrence of the quantum state output by the EPS.

Finally, we analyze the CAR data to characterize the power dependence of noise generated by the EPS. We prove that the accidental coincidences due to noise occur with a greater-than-quadratic dependence on the pump power, which is typical for Raman-scattered noise photons. We fit the data using an analytical model to show that, at least in some cases, self-phase modulation (SPM) of the pump contributes a significant amount of noise to our EPSs.

2. Experimental Procedure

2.1 Experimental Setup

The experimental setup includes a NuCrypt EPS, two PAs, and a CPDS. The EPS creates time–energy[7] entangled photon pairs through a $\chi^{(3)}$ nonlinear optical process known as four-wave mixing (FWM).[8,9] This results in two photons that are necessarily created at the same time and exhibit frequency (energy) correlations due to conservation of energy. Specifically, the sum of the energies of the two FWM photons must be equal to the sum of the energies of two photons from the pump laser, resulting in entangled photons with equal and opposite detuning from the pump frequency. This process occurs by pumping a dispersion-shifted fiber (DSF) with a 50-MHz pulsed laser operating at 193.1 THz. By arranging the DSF in a Sagnac loop with a polarization beam splitter (PBS) and setting the pump polarization to 45°, the EPS outputs a Bell state encoded in polarization, $|\Phi^+\rangle = \frac{1}{\sqrt{2}}(|HH\rangle + |VV\rangle)$.[10]

The signal and idler photons generated in the DSF have a broadband spectrum but are demultiplexed by the EPS into channels 26–29 and 33–36 on the 100-GHz-spaced International Telecommunication Union grid. Due to the energy correlations explained previously, the two photons of a FWM pair must be in channels that are symmetric about the pump channel (31) (i.e., entangled FWM pairs are generated in channels 26/36, 27/35, 28/34, and 29/33). The EPS also filters all other channels to remove various sources of noise photons. The PAs include various waveplates and a PBS in order to perform a measurement in any polarization basis, and the CPDS includes two InGaAs single-photon detectors (~20% detection efficiency) and the necessary electronics to perform coincidence measurements between the two detectors. A diagram of the setup is shown in Fig. 1 and detailed instructions of how to operate the NuCrypt EPS, PAs, and CPDS are included in Jones et al.[11]

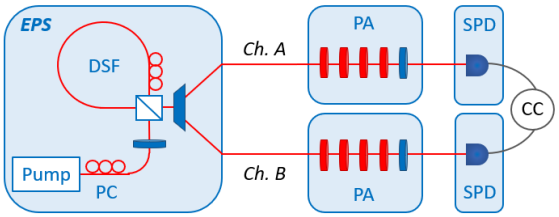

Fig. 1 Experimental diagram of the NuCrypt EPS, PAs, and SPDs. The EPS creates entangled photon pairs via the nonlinear optical process of FWM in the DSF. Quantum state tomography is performed using the PAs and SPDs.

2.2 Measuring Entangled Photon Spectra

In order to characterize the photons present in each channel pair, the spectrum of each channel should first be measured. Doing so determines the center frequency and bandwidth of each channel, both of which are important for modeling which types of photons are present in each channel. A Yokogawa AQ6370D optical spectrum analyzer (OSA) was used to measure the spectra of each output channel of the EPS. Before any measurements were taken, the internal components of the OSA were aligned, and a wavelength calibration was performed using the OSA's built-in calibration light source. After performing the alignment and calibration, the OSA was used in conjunction with a broadband source (BBS) (Thorlabs S5FC1550S-A2 fiber-coupled SLD source) in order to characterize the filter shape of each output channel of the EPS. The BBS was first connected directly to the OSA in order to directly measure the spectrum of the BBS. This provided a reference measurement that could later be used to accurately determine the filter shape of each EPS output channel. After measuring the BBS spectrum, the BBS was used as the input source for the EPS demultiplexer, and each output channel of the EPS was then connected directly to the OSA input. EPS output channel 26 was connected to and measured by the OSA first, and then all other channels (27–29 and 33–36) were connected and measured as well.

The data for each channel measurement was then imported into MATLAB, and the BBS spectrum was subtracted from the measured spectrum of each channel in order to properly normalize the transmission of each EPS channel. The BBS signal was subtracted because of the use of a logarithmic attenuation scale (decibels); however, the channel measurements would need to be divided by the BBS spectrum to

normalize the channel transmission values if a linear power-based scale was used. A plot showing the transmission of each EPS output channel is shown in Fig. 2. The peak transmission of each channel was –1.98 dB in channel 26, –1.27 dB in channel 27, –1.89 dB in channel 28, –2.21 dB in channel 29, –2.73 dB in channel 33, –3.22 dB in channel 34, –2.64 dB in channel 35, and –2.34 dB in channel 36.

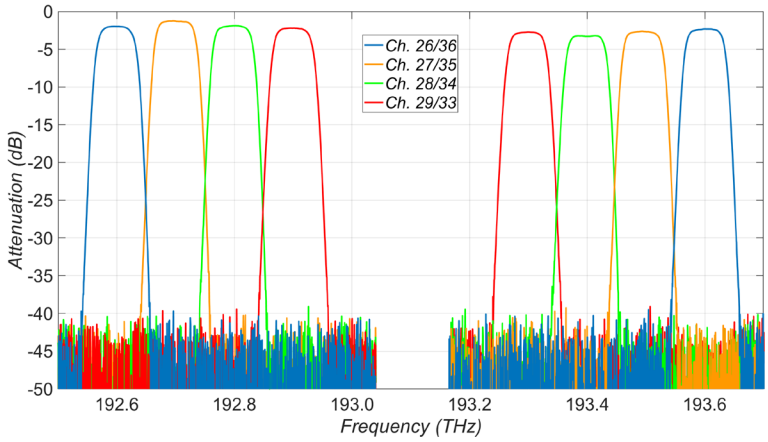

Fig. 2 Measurement of the filter shapes for the four channel pairs of an EPS using an OSA. The entangled photons have a broadband spectrum upon creation but are filtered into the four channel pairs shown here to reduce the amount of noise photons output by the source.

As seen in Fig. 2, channel pair 29/33 has the smallest detuning from the pump laser, which is located at 193.1 THz (channel 31). Due to the small detuning from the laser, we can predict that the presence of noise due to SPM of the pump would predominantly affect this channel pair. This is because SPM results in a spectral broadening of the pump laser, therefore causing leakage into the nearest channels.[12] On the other hand, channel pair 26/36 has the greatest detuning from the pump laser; therefore, these channels are expected to show the greatest influence of Raman-scattered noise photons. This is because Raman scattering increases as the detuning from the pump laser increases.[13,14]

2.3 Measuring the Coincidence to Accidental Ratio

Two uncorrelated light sources, each incident on a different detector, will still statistically result in some cases where both detectors simultaneously detect a photon (coincidence). This is known as an accidental coincidence and occurs with a probability equal to the product of the probabilities that each detector detects a photon within a given time. A useful metric for examining the performance of an EPS is the CAR. CAR is the ratio of the measured coincidences divided by the expected number of accidental coincidence counts of two detectors. For an EPS such as the NuCrypt EPS, a large CAR is typically indicative of a high degree of entanglement. Furthermore, examining the CAR as a function of the pump laser

attenuation (or power) can provide insight into the types of noise photons present in the system. This will be investigated in Section 3.1. However, CAR is not an entanglement metric, and entirely classical setups could be arranged to achieve very high CARs. For example, merely detecting the output of two laser pulses synchronized in time would result in a very large CAR.

The CAR was calculated for all four channel pairs of two different EPSs, one with an approximately 140-m-long DSF and one with an approximately 300-m-long DSF as a function of the pump attenuation/power. This was achieved by sending the output of each correlated channel pair to a CPDS and measuring the number of coincidence counts for a given measurement time. We used a measurement time of 2 s to detect the number of coincidences due to 100 million consecutive pump pulses (which have a 50-MHz repetition rate). We then divided the coincidences by the calculated number of expected accidental coincidences. The expected number of accidental coincidences was determined from measurements of the single counts of each detector. The number of counts measured by each detector divided by the number of measurement gates (i.e., the number of time windows in which the detector was open to the input light, which is equal to the number of pump pulses during the measurement time; see Jones et al.[11] for a detailed explanation) determines the probability of detection for that detector. By multiplying the detection probability of the two detectors by the number of measurement gates, we calculated the expected number of accidental coincidences. The pump attenuation was set by changing the power value entered in to the NuCrypt Entangled Photon Analyzer (EPA) software.

The CAR was initially measured for a maximum software-entered power of 3600, and subsequent measurements were performed at decreasing increments of 50 from 3600 to 3000 pump power. Additional measurements were also performed at increments of 25 between 3000 and 3200. All attenuation values were calculated by measuring the pump laser power at the output of the DSF. These powers were then converted to the attenuation of the pump laser relative to the maximum power (i.e., for a software-entered value of 3600). This resulted in measurements over a range of approximately 12 dB of attenuation (0 dB at a software-entered value of 3600 and ~12 dB at 3000).

2.4 Performing Quantum State Tomography

In addition to the time-energy entanglement of photon pairs generated by the NuCrypt EPS, the source is also constructed such that the photon pairs are entangled in polarization. Quantum state tomography[15] is the process by which the quantum state of a system (i.e., the photons output by the EPS) is characterized by

measuring the output of the system many times. For our EPS, performing tomography to determine the polarization entangled state requires measuring the amount of single and coincidence counts at each detector for 36 different settings of the two PAs. After taking these 36 measurements, a maximum likelihood estimation is performed to determine the density matrix that describes the quantum state output by the EPS.

Quantum state tomography was performed for all four channel pairs of one EPS as a function of the pump attenuation to determine the dependence of the quantum state and its entanglement quality on the pump attenuation. The measured density matrices and their concurrence were then evaluated to find evidence of additional noise photons in the system. See Section 3 of Jones et al.[11] for detailed instructions on how to perform quantum state tomography with the NuCrypt EPA software. Similar to our CAR measurements, tomography was initially performed with a maximum software-entered power of 3600, and subsequent tomography measurements were performed at decreasing increments down to 3000. Figure 3 shows an example density matrix and the corresponding entanglement metrics for a quantum state tomography performed with a NuCrypt EPS, PAs, and CPDS.

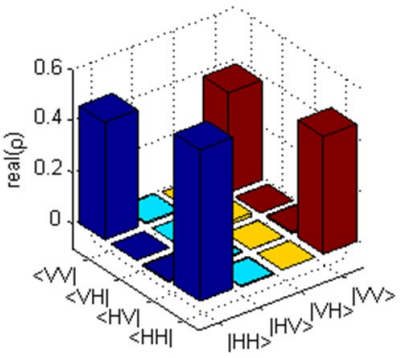


```
gates 100.000e6
coinc_max 1368
epspump_pwr 3250

figures       accid     dark     raw
of merit        sub      sub     data
-------------------------------------
fidelity:     0.950    0.858    0.848
tangle:       0.831    0.526    0.495
lin entropy:  0.100    0.316    0.338
concurrence:  0.912    0.725    0.704
purity:       0.925    0.763    0.747
```

Fig. 3 The density matrix and entanglement metrics calculated from a quantum state tomography performed for channel pair 27/35 of an EPS at a pump attenuation of –6.4 dB

3. Data and Analysis

3.1 Examining CAR for the Presence of Noise Due to Self-Phase Modulation

Figure 4 shows the CAR as a function of attenuation for all channel pairs of two NuCrypt EPSs. These data were measured using the process explained in Section 2.3. Figure 4a shows the CAR for the EPS with an approximately 140-m-long DSF, while Fig. 4b shows the CAR for the EPS with an approximately 300-m-long DSF.

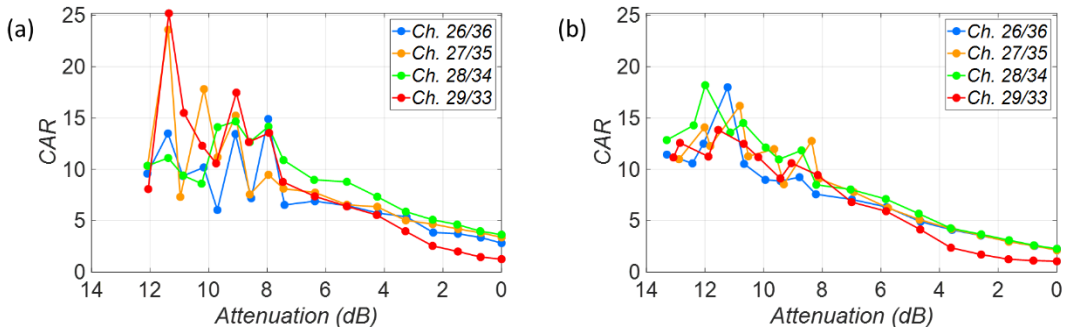

Fig. 4 CAR vs attenuation for four different channel pairs of a) an EPS with an approximately 140-m-long DSF and b) an EPS with an approximately 300-m-long DSF. For higher pump powers (less attenuation), the CAR decreases due to an increased amount of noise photons generated by the source. The greatest decrease in CAR occurs for the photons (ch. 29/33) nearest the pump frequency—a sign of noise photons due to SPM of the pump.

As stated earlier in Section 2.3, the dependence of CAR on power can provide insight into the types of noise photons present in the system. Previous characterization[16,17] of our EPSs has resulted in a clear understanding of two types of photons generated by the EPS—that is, entangled photons created via FWM and Raman-scattered noise photons. However, there is reason to suspect that a non-negligible amount of noise photons may also be output by the EPS due to SPM of the pump laser.[12] Similar to FWM, SPM is also a $\chi^{(3)}$ nonlinear optical process that occurs in systems such as our EPS. SPM results in a spectral broadening of the pump laser, therefore potentially resulting in the leakage of additional noise photons into the entangled photon spectral bands (i.e., into channels 26–29 and 33–36).

Photon pairs created by FWM, such as the entangled pairs generated by the EPS, are created as a quadratic function of power, $\mu \sim a\, P^2$, where μ is the probability per pump pulse that two photons from the pump pulse are converted into an entangled pair via FWM, a is a constant, and P is the pump power. Since both photons generated by FWM are necessarily created at the same time, the probability of a single photon detection and a coincident detection of both photons are both quadratic in power. Meanwhile, Raman-scattered photons are linear in power, $r_i \sim b_i\, P$, where r_i is the probability per pump pulse that a noise photon is generated in channel i due to Raman scattering and b_i is a constant. However, Raman-scattered photons generated in each channel are created independently, so the probability of a coincidence due to two Raman photons (one source of accidental coincidences) is the product of their individual probabilities, which also happens to be quadratic in power like coincidences due to FWM. Meanwhile, similar to entangled photons created via FWM, SPM photons are also quadratic in power, $\sigma_i \sim c_i\, P^2$, where σ_i is the probability per pump pulse that a noise photon is generated in channel i due to SPM-induced broadening of the pump, and c_i is a

constant. Furthermore, similar to noise photons due to Raman scattering, the presence of a noise photon due to SPM in one channel is independent of the presence of a photon due to SPM in the other, so the probability of an accidental coincidence due to two SPM photons is the product of their individual probabilities ($\sim P^4$).

Therefore, since coincidences of entangled pairs and accidental coincidences of Raman photons are both quadratic, CAR is expected to be constant as a function of power. However, as seen in Fig. 4, CAR decreases as attenuation increases, a sign of accidentals occurring with a dependence greater than P^2, indicating the presence of an additional source of noise photons. Furthermore, this decrease in CAR is most dramatic for channels 29/33, the channels with the smallest detuning from the pump laser, evidence of an effect that is a function of detuning from the pump frequency. The greater-than-P^2 dependence combined with the fact that the least-detuned channels experience the greatest drop in CAR (i.e., the greatest increase in noise photons) provide evidence that there are indeed noise photons due to SPM present in the system. To verify this, we performed a nonlinear regression on the measured CAR values using the MATLAB *fitnlm* function.

Given the evidence of SPM, we fit our data to a model that includes three types of photons present in the system. First, we assume that all coincidences due to entangled pairs are created by FWM. Next, we assume that all accidental coincidences are due to either coincidental detections of two independent Raman-scattered photons or coincidental detections of two independent SPM photons. The accidental coincidences due to Raman scattering and SPM both will actually be detected; therefore, they must be included in both the numerator and denominator of the CAR. Given the power dependence of coincidences due to each of these three effects, the CAR can be expressed as

$$CAR = \frac{C_{FWM} + A_R + A_{SPM}}{A_R + A_{SPM}} = \frac{\alpha P^2 + \beta P^2 + \gamma P^4}{\beta P^2 + \gamma P^4} = \frac{(\alpha + \beta) + \gamma P^2}{\beta + \gamma P^2}, \quad (1)$$

where C_{FWM} is the number of coincidences due to FWM photon pairs, A_R is the number of accidental coincidences due to Raman-scattered photons, A_{SPM} is the number of accidental coincidences due to SPM, α is a coefficient that determines the amount of FWM pairs, β is a coefficient that determines the amount of accidental coincidences due to Raman-scattered photons, and γ is a coefficient that determines the amount of accidental coincidences due to SPM photons. Since SPM is negligible at low power, we make the approximation that CAR is equal to the sum of coincidences due to FWM and accidental coincidences due to Raman scattering divided by the amount of accidentals due to Raman-scattered photons

(i.e., $CAR_0 = (\alpha + \beta)/\beta$) at low powers. After dividing both the numerator and denominator by $(\alpha + \beta)$, substituting for CAR_0, and performing some simple algebra, the CAR can be expressed as

$$CAR = 1 + \frac{1 - \frac{1}{CAR_0}}{\frac{1}{CAR_0} + \gamma_{\alpha\beta} P^2}. \quad (2)$$

As the low-power measurements are rather noisy due to a decreased number of total counts, we set CAR_0 equal to the average CAR of the five lowest-power measurements for each channel pair. Finally, we perform the fit to determine the remaining free parameter, $\gamma_{\alpha\beta} = \gamma/(\alpha + \beta)$.

The resulting fits for the CAR values measured for the channel 29/33 data of each EPS are shown in Fig. 5. The function given in Eq. 2 fits the data rather nicely with a calculated value of $\gamma_{\alpha\beta} = 6.97 * 10^{-5}$ and a coefficient of determination of $R^2 = 0.97$ for the EPS with an approximately 140-m-long DSF. Likewise, the data for the EPS with an approximately 300-m-long DSF are fit with a calculated value of $\gamma_{\alpha\beta} = 1.84 * 10^{-4}$ and a coefficient of determination of $R^2 = 0.97$. The relative amount of noise due to SPM (i.e., $\gamma_{\alpha\beta}$) appears to increase with the length of the DSF of the EPS; however, further investigation is required to fully characterize how the length of DSF affects the amount of noise photons generated.

The data for channel pair 28/34 can be fit reasonably well by Eq. 2 ($R^2 = 0.94$ for the EPS with the shorter DSF and $R^2 = 0.95$ for the longer DSF); however, the remaining channels cannot be accurately fit, resulting in significantly smaller R^2 values and curves that clearly do not visually fit the data. The successful fit of the channel 29/33 and 28/34 data to Eq. 2 confirms the presence of noise photons that are generated as a quadratic function of power (therefore, accidental coincidences due to these photons scale as $\sim P^4$). Furthermore, the fact that the least-detuned channels (29/33) can be accurately fit by Eq. 2, but the most-detuned channels cannot, provides evidence that these additional noise photons are indeed due to SPM. Further analysis is also required to accurately model the behavior of the channels that could not be accurately fit by Eq. 2.

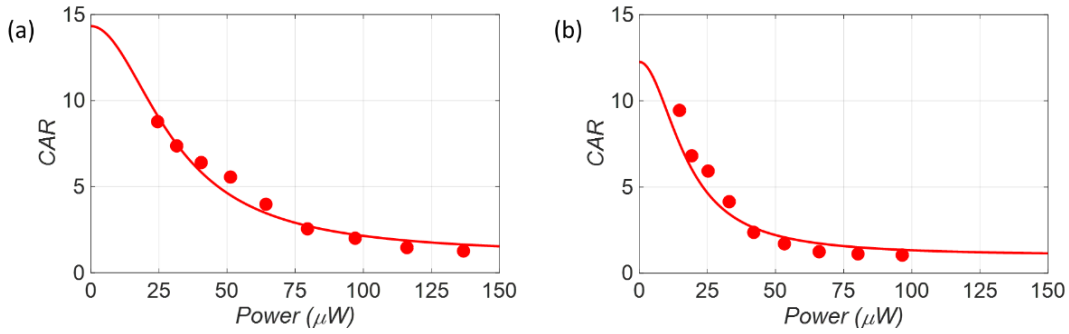

Fig. 5 CAR vs. power for channel pair 29/33 of a) an EPS with an approximately 140-m-long DSF and b) an EPS with an approximately 300-m-long DSF. The curves are the result of fitting Eq. 2 to the measured CAR values.

3.2 Concurrence

Concurrence is one of many entanglement metrics that can be calculated from the density matrix, and it is often used to characterize entanglement quality in many practical situations, such as when photons experience polarization mode dispersion[18-21] and polarization dependent loss[3,22,23] in optical fibers. As noted in Section 2.4, the concurrence can also be examined to find evidence of additional noise photons output by the source. A concurrence of 1 corresponds to a maximally entangled state, and a concurrence of 0 corresponds to a separable state (no entanglement). Concurrence was calculated for all tomography measurements explained in Section 2.4 in order to characterize the entanglement quality of each channel pair as a function of the pump attenuation. Figure 6 shows the raw (four lower curves) and accidental-subtracted (four upper curves) concurrence values for each channel pair of the EPS with an approximately 140-m-long DSF. The raw concurrence is determined from the density matrix calculated from each of the 36 tomography measurements without any additional processing. The raw concurrence quantifies the entanglement quality of the actual state output by the EPS, including all noise photons. On the other hand, the accidental-subtracted density matrix and concurrence approximate the quantum state of the entangled photons without the additional noise photons generated by the EPS. These are determined by subtracting the accidental counts from each of the 36 tomography measurements before calculating the density matrix.

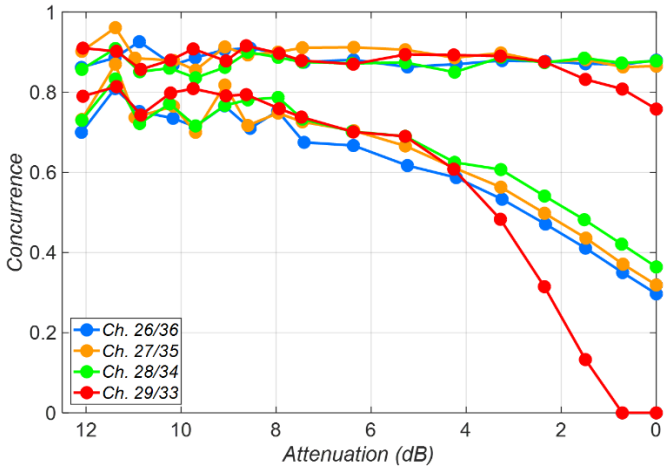

Fig. 6 Accidental subtracted concurrence (upper four curves) and raw concurrence (lower four curves) vs. pump laser attenuation for four different channel pairs of the EPS with an approximately 140-m-long DSF. Similar to the CAR plots in Fig. 4, the concurrence also decreases for less attenuation. Furthermore, the greatest decrease in concurrence also occurs for channel pair 29/33, another sign of the presence of noise photons due to SPM.

As expected, the accidental-subtracted concurrence is virtually constant as a function of power since the counts due to accidental coincidences (i.e., due to noise photons) are subtracted from the tomography measurements before calculating the density matrix. However, the raw concurrence decreases as the attenuation decreases (power increases) due to the increased amount of noise photons generated by the source. Furthermore, similar to the CAR for channel 29/33, the concurrence of photons in channel 29/33 also decreases significantly more than the other channels as a function of power. This can also be attributed to the generation of noise photons due to SPM in the EPS.

4. Conclusions

In order to effectively use an EPS for quantum networking applications, the user must have knowledge of the noise photons output by the source. In this technical report, we performed various important measurement processes required to operate and characterize the behavior of our EPS. We characterized the spectrum of entangled photons output by the EPS, measured the CAR of light output by the EPS, performed quantum state tomography, and analyzed the concurrence of the quantum state output by the EPS. Finally, we analyzed the CAR data and performed a nonlinear regression with a model including noise photons due to SPM in order to characterize the noise generated by the EPS. This fit confirmed that there is a significant amount of accidental coincidences due to noise that occur with a P^4 dependence on the pump power. Furthermore, the fact that only the least-detuned channels can be accurately fit by our model provides evidence that these

photons are generated by SPM of the pump. Additional analysis of the concurrence of the polarization-entangled state generated by the EPS further supports our claim that noise photons due to SPM are present in the system. Further investigation is required in order to model the behavior of the remaining EPS output channels and to fully characterize the effect of the DSF length on the performance of the EPS.

5. References

1. Kimble H. The quantum internet. Nature. 2008;453:1023–1030.
2. Van Meter R. Quantum Networking. Hoboken (NJ): John Wiley & Sons; 2014.
3. Jones DE, Kirby BT, Brodsky M. Tuning quantum channels to maximize polarization entanglement for telecom photon pairs. NPJ Quantum Int. 2018;4:58.
4. Duan L-M, Lukin M, Cirac J, Zoller P. Long-distance quantum communication with atomic ensembles and linear optics. Nature. 2001;414:413–418.
5. Munro W. Harrison K, Stephens A, Devitt S, Nemoto K. From quantum multiplexing to high-performance quantum networking. Nat Photonics. 2010;4:792–796.
6. NuCrypt, LLC. Product overview: quantum optical instrumentation (online). [accessed 2017 July]. http://www.nucrypt.net/quantum-optical-instrumentation.html
7. Franson JD. Bell inequality for position and time. Phys Rev Lett. 1989;62:2205–2208.
8. Fiorentino M, Voss PL, Sharping JE, Kumar P. All-fiber photon-pair source for quantum communications. IEEE Photon Technol Lett. 2002;14:983–985.
9. Inoue K. Four-wave mixing in an optical fiber in the zero-dispersion wavelength region. J Lightwave Technol. 1992;10:1553–1561.
10. Wang SX, Kanter GS. Robust multiwavelength all-fiber source of polarization-entangled photons with built-in analyzer alignment signal. IEEE J Sel Top Quantum Electron. 2009;15:1733–1740.
11. Jones DE, Weninger D, Brodsky M. Setting single photon detectors for use with an entangled photon distribution system. Aberdeen Proving Ground (MD): Army Research Laboratory (US); 2017 Dec. Report No.: ARL-TR-8229.
12. Ma X, Yang L, Guo X, Li X. Generation of photon pairs in dispersion shift fibers through spontaneous four wave mixing: influence of self-phase modulation. Opt Commun. 2011;284:4558–4562.
13. Newbury NR. Pump-wavelength dependence of Raman gain in single-mode optical fibers. J Lightwave Technol. 2003;21:3364.

14. Voss PL, Kumar P. Raman-noise-induced noise-figure limit for $\chi^{(3)}$ parametric amplifiers. Opt Lett. 2004;29:445–447.

15. Altepeter JB, Jeffrey ER, Kwiat PG. Photonic state tomography. In: Berman PR, Lin CC, editors. Advances in atomic, molecular, and optical physics. Cambridge (MA): Elsevier; 2005. p. 105–159.

16. Jones DE, Kirby BT, Brodsky M. Joint characterization of two single photon detectors with a fiber-based source of entangled photon pairs. Frontiers in Optics 2017. Washington (DC): Optical Society of America; 2017. Paper No.: JW4A.37.

17. Jones DE., Kirby BT, Brodsky M. In-situ calibration of fiber-optics entangled photon distribution system. In: Proc. IEEE Photonics Society Summer Topical Meeting Series; 2017; p. 123–124.

18. Brodsky M, Frigo NJ, Boroditsky M, Tur M. Polarization mode dispersion of installed fibers. J Light Technol. 2006;24:4584–4599.

19. Antonelli C, Shtaif M, Brodsky M. Sudden death of entanglement induced by polarization mode dispersion. Phys Rev Lett. 2011;106:080404.

20. Brodsky M, George EC, Antonelli, C, Shtaif M. Loss of polarization entanglement in a fiber-optic system with polarization mode dispersion in one optical path. Opt Lett. 2011;36:43–45.

21. Shtaif M, Antonelli C, Brodsky M. Nonlocal compensation of polarization mode dispersion in the transmission of polarization entangled photons. Opt Express. 2011;19:1728–1733.

22. Jones DE, Kirby BT, Brodsky M. Polarization dependent loss in optical fibers-does it help or ruin photon entanglement distribution? Optical Fiber Communication Conference Postdeadline Papers. Washington (DC): Optical Society of America; 2018. Paper No.: Th4B.1.

23. Kirby BT, Jones DE, Brodsky M. Effect of polarization dependent loss on the quality of transmitted polarization entanglement. J Light Technol. 2019;37:95–102.

List of Symbols, Abbreviations, and Acronyms

BBS	broadband source
CAR	coincidence to accidental ratio
CC	coincidence counting electronics
CPDS	correlated photon detection system
DSF	dispersion-shifted fiber
EPA	Entangled Photon Analyzer
EPS	entangled photon source
FWM	four-wave mixing
OSA	optical spectrum analyzer
PA	polarization analyzer
PBS	polarization beam splitter
PC	polarization controller
SLD	superluminescent diode
SPD	single photon detector
SPM	self-phase modulation

1 (PDF)	DEFENSE TECHNICAL INFORMATION CTR DTIC OCA
1 (PDF)	CCDC ARL FCDD RLD CL TECH LIB
1 (PDF)	GOVT PRINTG OFC A MALHOTRA
1 (PDF)	CCDC ARL FCDD RLC NT D JONES